Self-regulated propagation of intense infrared pulses in elongated soft-x-ray plasma amplifiers

Eduardo Oliva, Adrien Depresseux, Fabien Tissandier, Julien Gautier, Stéphane Sebban, Gilles Maynard

Self-regulated propagation of intense infrared pulses in elongated soft-x-ray plasma amplifiers

Eduardo Oliva,[1,*] Adrien Depresseux,[2] Fabien Tissandier,[2] Julien Gautier,[2] Stéphane Sebban,[2] and Gilles Maynard[1]
[1]*Laboratoire de Physique des Gaz et des Plasmas, Université Paris Sud, CNRS, UMR8578, 91405 Orsay, France*
[2]*Laboratoire d'Optique Appliquée, ENSTA ParisTech, École Polytechnique ParisTech, CNRS, UMR7639, 91761, Palaiseau, France*
(Received 7 April 2015; published 26 August 2015)

Increasing the electron density of collisionally pumped plasma-based soft-x-ray lasers offers promising opportunities to deliver ultrashort pulses. However, strong nonlinear effects, such as overionization-induced refraction and self-focusing, hinder the propagation of the laser beam and thus the generation of elongated volume of lasing ions to be pumped. Using a particle-in-cell code and a ray-tracing model we demonstrate that optically preformed waveguides allow for addressing those issues through a self-regulation regime between self-focusing and overionization processes. As a result, guiding intense pulses over several millimeters leads to the implementation of saturated plasma amplifiers.

DOI: 10.1103/PhysRevA.92.023848 PACS number(s): 42.15.Dp, 42.55.Vc, 52.38.Hb, 52.38.Ph

I. INTRODUCTION

The development and the applications of ultraintense and ultrashort radiation from XUV to x rays have experienced a dramatic expansion in the past few years with the emergence of free-electron lasers (FELs). The excellent optical properties of these sources opened new ways in such important fields as material science and biology by means of coherent imaging (diffraction [1] and holography [2]). However, since few FELs are available, the number of projects that can be carried out in these facilities and the allotted beam time are limited. The access to complementary small-scale facilities delivering x-ray pulses not only would ensure the conduction of experiments that do not need the extreme FEL performances, but also would help to prepare and increase the success of FELs experiments.

Among these complementary sources, plasma-based seeded soft-x-ray lasers (SXRL) [3,4] offer a promising approach. These sources demonstrated energetic picosecond pulses [5] with full spatial and temporal coherences and good wavefronts [6]. In addition to this, different techniques to deliver subpicosecond pulses [7–10] have been proposed. Most of these techniques rely on increasing the density of the plasma amplifier, broadening the lasing transition linewidth [11].

In order to get optimized spatial and temporal properties, the SXRL should reach the saturated amplification regime. This requires achieving plasma amplifiers of a few millimeters length. Elongated optical field ionized [12,13] plasmas filled with lasing ions are generated focusing an ultrashort intense infrared (IR) pulse onto a target. When the plasma is created from a solid target, the IR pump beam takes advantage of the refraction induced by the density gradient to efficiently deposit the laser energy at the optimum density [14]. In the case of a gas target, the pump pulse has to propagate through the full length of the amplifier, which becomes a quite problematic issue when the electron density is increased (i.e., $n_e \approx 10^{19}$ cm^{-3}).

Intense IR pulses can be guided over several Rayleigh lengths using a preformed plasma waveguide. In Ref. [15], the propagation of a moderate intensity ($I = 2.5 \times 10^{15}$ W cm^{-2}) IR pulse through a partially ionized hydrogen plasma channel is studied. The total density has a truncated parabolic profile with $n_0 = 5 \times 10^{17}$ cm^{-3} at the center and 0.89×10^{18} cm^{-3} at $r = 66$ μm. It is found that the performance of the waveguide depends strongly on the initial degree of ionization. A high initial degree of ionization is needed in order to guide the pulse, thus hinting that refraction plays a fundamental role. Guiding at moderate intensities (10^{13}–10^{14} W cm^{-2}) was achieved in argon, nitrogen, and xenon using plasma channels [16]. Guiding at higher intensities ($I = 4 \times 10^{18}$ W cm^{-2}) using a capillary discharge waveguide filled with hydrogen has also been experimentally demonstrated in relation with laser wakefield acceleration of relativistic electrons [17].

The situation is much more complex in dense plasma-based soft-x-ray lasers. In these amplifiers, an intense ($I > 10^{18}$ W cm^{-2}) IR pulse must propagate over several millimeters or even centimeters of a partially ionized high-Z (i.e., krypton) plasma [18,19]. At such high intensities, further ionization of the plasma is not uniform but strongly depends on the IR beam intensity [20,21]. Therefore, the physics of the propagation becomes highly nonlinear, the initial electron-density profile inside the channel being strongly perturbed by the laser beam. Note also that nonlinear relativistic effects may also play a role, leading to the well-known relativistic self-focusing effect [22]. Relativistic self-focusing appears when the beam power is higher than the threshold power [23] $P_{\mathrm{th}}(W) \approx 1.7 \times 10^{10} \frac{n_c}{n_e}$, where n_c is the plasma critical density and n_e is the electron density. Thus, new challenges arise when modeling these kinds of waveguides.

In this paper we analyze this propagation regime (intense IR pulse through a dense plasma channel that can be multiply ionized) using the particle-in-cell (PIC) code WAKE-EP (extended performances) [24], an upgrade of the quasistatic two-dimensional axisymmetric particle code WAKE [25]. The study is carried out in the case of Kr^{8+} plasma amplifiers [26]. We will show that a self-regulating mechanism (with similarities with laser filamentation of intense IR pulses propagating through gases, liquids, and solids [27]) appears in which overionization-induced refraction (due to relativistic self-focusing) is compensated by plasma guiding. The pump pulse waveguiding combined with the prevalence of Kr^{8+}

*Present address: Instituto de Fusión Nuclear, Universidad Politécnica de Madrid, 28006, Madrid, Spain; eduardo.oliva@upm.es

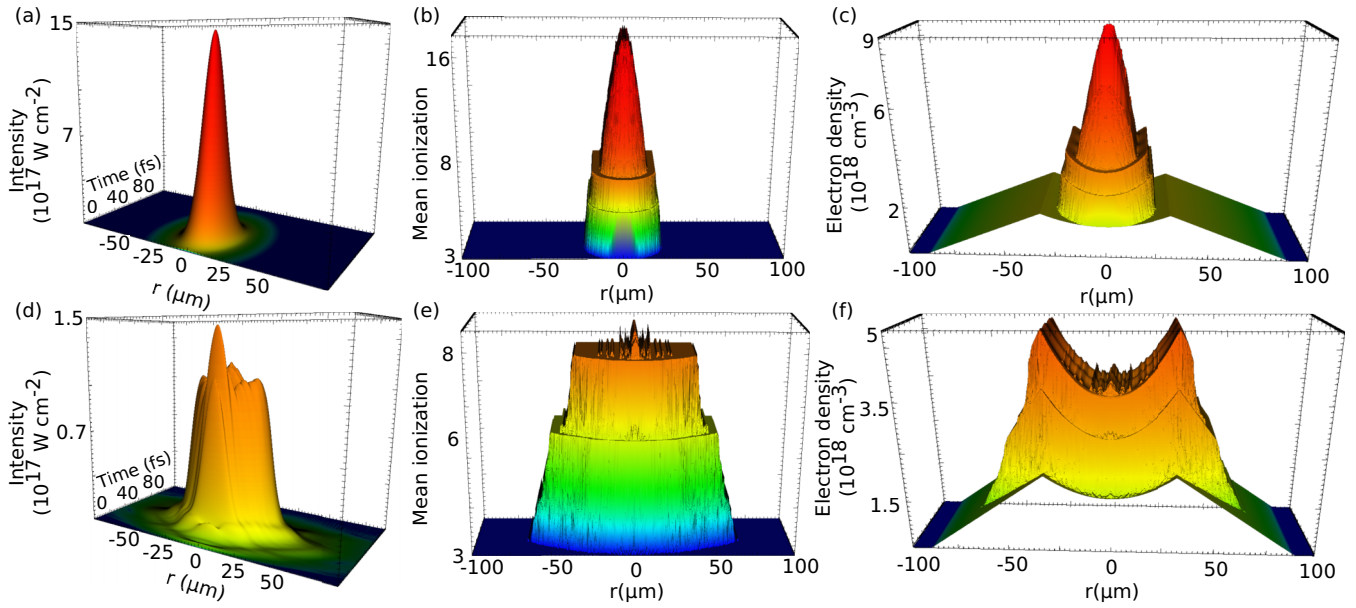

FIG. 1. (Color online) (a) Intensity, (b) mean ionization, and (c) electron density at $z = 0$. (d) Intensity, (e) mean ionization, and (f) electron density at $z = 1.5Z_R$. $Z_R = 0.0725$ cm. The temporal scale is the same in all six figures, but it is only depicted in (a) and (d) for the sake of visualization.

lasing ions due to its superior stability allows efficiently filling plasmas of several Rayleigh lengths (more than ten). This opens the way for centimeter-scale dense soft-x-ray amplifiers while promising ultrashort ($\Delta t \approx 100$-fs) pulses.

II. SIMULATIONS

In this paper we model the propagation of an intense IR pulse through a Kr^{3+} plasma channel created with the ignitor-heater technique using an axicon lens [19,28]. The IR pulse should be efficiently guided through the plasma to fill properly the whole plasma length with Kr^{8+} ions and to generate a population inversion via collisions of hot electrons with lasing ions.

The parameters of the simulations are chosen to match recent experimental conditions [18,29,30]. The IR laser pulse $\lambda = 800$ nm, $E = 250$ mJ, $\Delta t = 30$ fs FWHM was focalized into a 16 μm focal spot ($I \approx 1.4 \times 10^{18}$ W cm^{-2}) at the entrance of the preformed plasma channel. The plasma channel density has a truncated parabolic radial shape, decreasing linearly afterwards,

$$N_n(r) = N_0\left(1 + \frac{r^2}{R_0^2}\right), \quad r < R_c, \tag{1}$$

$$N_n(r) = N_0\left(1 + \frac{R_c^2}{R_0^2}\right)\left(\frac{R_v - r}{R_v - R_c}\right), \quad R_c < r < R_v, \tag{2}$$

where N_n is the atomic density and N_0, R_0 are the parameters of the parabola [N_0 being the density at $r = 0$ and R_0 being the radial coordinate where $N_n(R_0) = 2N_0$]. R_c is the radius of the channel where the density attains its maximum, and R_v is the point where vacuum starts. We assume that the plasma is initially ionized three times (Kr^{3+}), and thus the initial electron density is $n_e(r, t = 0) = 3N_n(r)$. In this article, these parameters are adjusted to experimental data [29,30] taking the values $R_0 = 50.6$, $R_c = 32.0$, and $R_v = 90.0$ μm. Different values of the electron density at the center of the unperturbed channel, ranging from $n_e(r = 0, t = 0) = 1.4 \times 10^{16}$ to $n_e(r = 0, t = 0) = 4.1 \times 10^{18}$ cm^{-3}, were explored to ascertain the role played by the density.

Figure 1(a) shows the initial intensity profile of the laser pulse when entering the plasma channel with an initial electron density of $n_e(r = 0, t = 0) = 1.4 \times 10^{18}$ cm^{-3}. The intensity is so high that the mean ionization [shown in Fig. 1(b)] reaches $\bar{Z} = 16$, which is much greater than the desired $\bar{Z} = 8$ that roughly corresponds to the lasing ion Kr^{8+}. This overionization induces a steep electron-density gradient at the center of the channel, depicted in Fig. 1(c). This overionization-induced gradient strongly defocuses the IR beam, thus overcoming the guiding of the plasma channel.

After one and a half Rayleigh lengths, the maximum intensity has been reduced one order of magnitude [Fig. 1(d)] to a value that cannot produce the Kr^{9+} ion. Thus, most of the channel is composed of Kr^{8+} [Fig. 1(e)]. This ion proliferates because of its increased stability deriving from its closed subshell. At this moment, the defocusing gradients have disappeared [Fig. 1(f)], and the plasma channel starts guiding the pulse as Fig. 2(a) shows. The intensity of the pulse increases steadily due to the guiding effect until the self-focusing threshold is attained. From this point ($z \approx 3Z_R$), the intensity of the pulse increases faster [Fig. 2(a)] and produces an overionization at the center of the plasma [Fig. 2(b)], triggering refraction effects that defocus the beam which then gets reflected onto the density gradient of the waveguide. In this way, there is a competition between overionization refraction and refocusing from the waveguide density gradient, which leads to an elongated gain medium filled with lasing ions over its whole length as shown in Fig. 2(b). This mechanism allows for the propagation of a pulse intense enough to produce the Kr^{8+} ion but not the Kr^{9+} along more than ten Rayleigh lengths as Fig. 2(b) depicts.

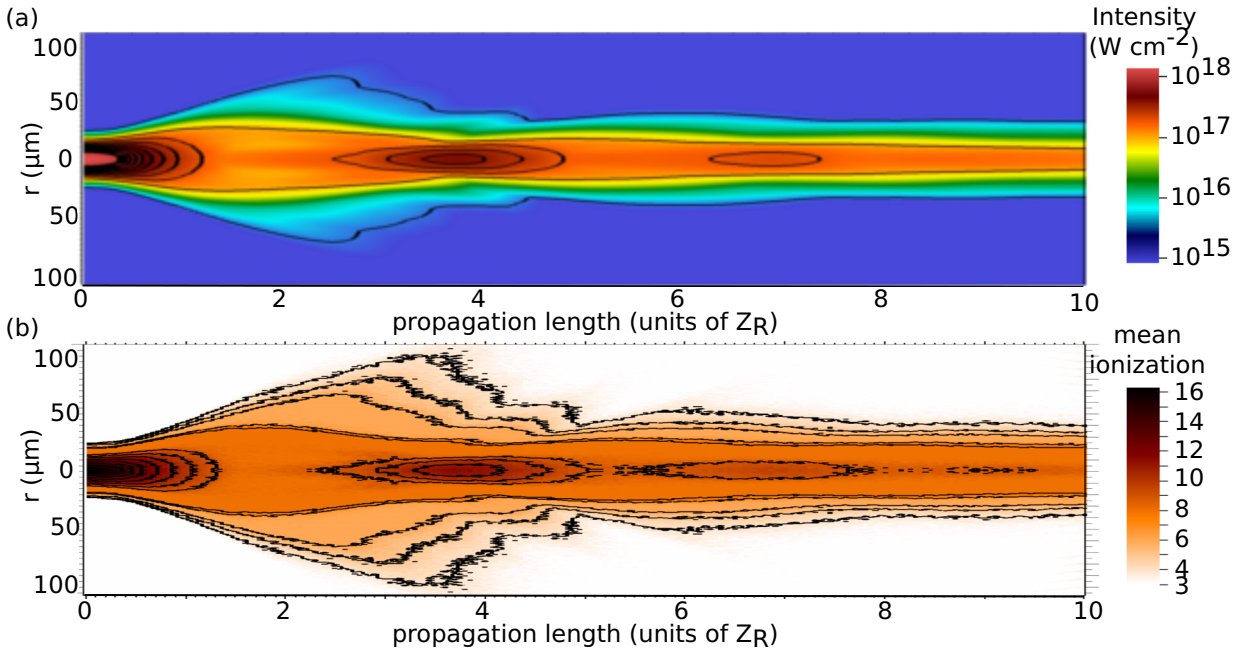

FIG. 2. (Color online) (a) Maximum intensity along the plasma channel. (b) Mean ionization along the plasma channel. $Z_R = 0.0725$ cm.

III. RAY-TRACING MODEL

The predominance of channel guiding, overionization defocusing, or diffraction can be ascertained with a simple model. In an ideal case of paraxial approximation, the ray trajectories of a Gaussian beam diffracting and propagating through a parabolic channel are easily computed [31]. When the electron-density profile of the channel is

$$n_e(r) = n_{e1}\left(1 + \frac{r^2}{r_{e1}^2}\right), \quad 0 < r < R_c, \tag{3}$$

they are given by

$$w_d(z) = w_0\sqrt{1 + \frac{z^2}{Z_R^2}}, \tag{4}$$

$$w_c(z) = w_0 \cos\left(\left[\frac{n_{e1}}{n_c}\right]^{1/2}\frac{z}{r_{e1}}\right), \tag{5}$$

where w_0 denotes the initial radial coordinate of the ray, n_c is the critical density, n_{e1} is the density at $r = 0$, and r_{e1} is the coordinate where $n_e(r_{e1}) = 2n_{e1}$. These parameters are depicted in Fig. 3.

The condition for perfect guiding is that the first derivative of the trajectory is zero (i.e., the rays are parallel to the axis). Then, when our system is near perfect guiding, we can perform a Taylor expansion of the trajectories,

$$w_d(z) \approx w_0\left[1 + \frac{1}{2}\frac{z^2}{Z_R^2}\right], \tag{6}$$

$$w_c(z) \approx w_0\left[1 - \frac{1}{2}\frac{z^2}{Z_1^2}\right], \tag{7}$$

where $Z_1 = r_{e1}\sqrt{\frac{n_c}{n_{e1}}}$ is the channel refraction characteristic length.

Guiding is achieved when the sum of the second-order terms in both equations is zero, obtaining the same criterion given in Ref. [16] but in terms of the parameters of the channel and the Rayleigh length,

$$Z_R = Z_1. \tag{8}$$

The criterion given by Eq. (8) is a balance between two characteristic lengths, diffraction (Z_R) and the deviation induced by the parabolic channel (Z_1). Whether diffraction

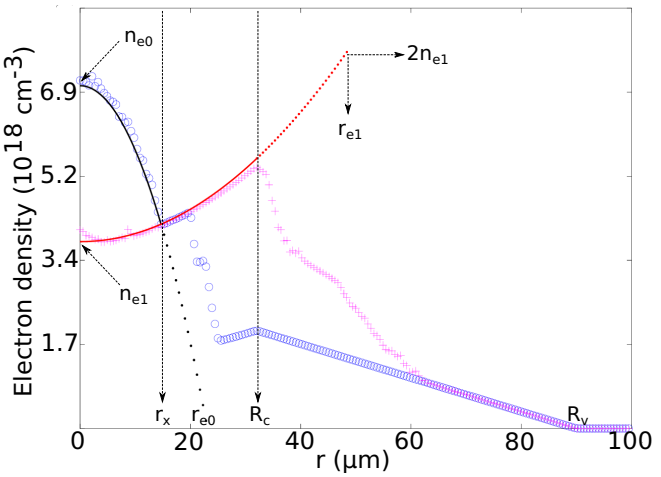

FIG. 3. (Color online) Parameters for the two-parabola ray-tracing model [Eqs. (9) and (3)]. The electron-density radial profile at $z = 0$ (blue circles) and $z = 1.5Z_R$ (magenta crosses) as given by the PIC code are depicted. Continuous lines (red and black) represent the parabolas that approximate the computed electron-density profile.

TABLE I. Electron density (cm^{-3}) at the center of the unperturbed Kr^{3+} channel (first row). Refraction characteristic length (cm) of the ideal guiding Kr^{8+} channel (second row) and of the overionized profile at the center of the channel (third row). The Rayleigh length is $Z_R = 0.0725$ cm. The shortest characteristic length (Z_R, Z_1, Z_0) determines which mechanism dominates: diffraction, channel guiding, or overionization-induced refraction, respectively.

$n_{e1}^{3+}(\times 10^{17})$	0.14	0.57	1.3	2.3	3.6	5.2	7.0	14.3	41.4
Z_1	1.1	0.54	0.36	0.27	0.21	0.18	0.15	0.11	0.06
Z_0	0.33	0.17	0.11	0.08	0.07	0.06	0.05	0.04	0.02

or refraction predominates depends on which of these lengths is shorter.

After interaction with the intense IR pulse, the plasma is ionized to Kr^{8+} in most of the channel and to higher ionization states at the central part where the intensity of the IR pulse is stronger as shown in Fig. 2(b). The overionized region at the center of the channel is adjusted by Eq. (9) (black line in Fig. 3),

$$n_e(r) = n_{e0}\left(1 - \frac{r^2}{r_{e0}^2}\right), \quad r < r_x, \tag{9}$$

$$n_e(r) = n_{e1}\left(1 + \frac{r^2}{r_{e1}^2}\right), \quad r_x < r < R_c. \tag{10}$$

The parameters of the parabola are $n_{e0} = n_e(0)$ and r_{e0}, which is the coordinate where $n_e(r_{e0}) = 0$. Both parabolas intercept at r_x. All these parameters are depicted in Fig. 3. The increasing parabola, adjusted by Eq. (10) (red line in Fig. 3) models the Kr^{8+} plasma channel since the low intensity region of the radial profile of the pulse is intense enough to attain this level of ionization [as shown in Fig. 2(b)]. The characteristic length of the defocusing induced by this overionization $Z_0 = r_{e0}\sqrt{\frac{n_c}{n_{e0}}}$ is obtained Taylor expanding the corresponding hyperbolic cosine ray trajectory as done with Eq. (5).

Table I shows the refraction characteristic lengths of the focusing induced by the plasma channel and defocusing induced by overionization after interaction with the IR pulse. For lower electron densities, diffraction is the predominant effect. Only in the densest cases $Z_1 \approx Z_R$, which is the condition for an efficient guiding. However, as the third row of Table I shows, in these cases overionization-induced refraction dominates both guiding and diffraction $(Z_0 < Z_1, Z_R)$. The predominance of this defocusing refraction implies that the criterion given by Eq. (8) is no longer valid. Since we are interested in the densest cases where refraction predominates, ray-tracing techniques can be used to study the evolution of the pulse as refraction dominates diffraction.

A ray starting parallel to the Z axis at $r = \rho_0 < r_x$ will follow this trajectory [31],

$$r(z) = \begin{cases} \rho_0 \cosh\left[\frac{z}{Z_0}\right], & r < r_x, \\ \rho_1 \cos\left[\frac{z}{Z_1} + \phi_1\right], & r > r_x, \end{cases} \tag{11}$$

where ρ_1 and ϕ_1 are chosen so as to ensure the continuity of the trajectory and its first derivative. Defining $z_c = Z_0 \cosh^{-1}\frac{r_x}{\rho_0}$ [i.e., $r(z_c) = r_x$] we can compute the parameters as

$$\phi_1 = \arctan\left(-\frac{Z_1}{Z_0}\tanh\frac{z_c}{Z_0}\right) - \frac{z_c}{Z_0},$$

$$\rho_1 = \frac{\rho_o \cosh\frac{z_c}{Z_0}}{\cos\left[\arctan\left(-\frac{Z_1}{Z_0}\tanh\frac{z_c}{Z_0}\right)\right]}.$$

A ray will be confined in the channel if its maximum radial deviation ρ_1 is smaller than the channel radius R_c,

$$\rho_1 = \frac{\rho_0 \cosh\frac{z_c}{Z_0}}{\cos\left[\arctan\left(-\frac{Z_1}{Z_0}\tanh\frac{z_c}{Z_0}\right)\right]} \leqslant R_c.$$

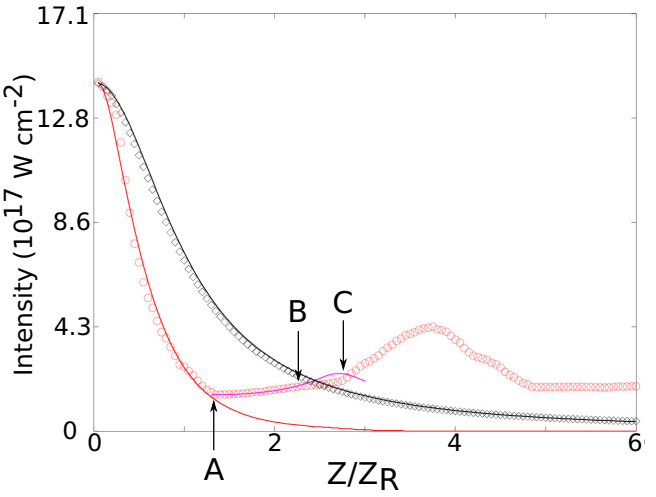

FIG. 4. (Color online) Maximum intensity as given by the PIC simulation for $n_{e1} = 1.4 \times 10^{16}$ cm^{-3} (black diamonds) and $n_{e1} = 1.4 \times 10^{18}$ cm^{-3} (red circles) compared with the propagation of a Gaussian beam in vacuum (black line) and our ray-tracing model (red and magenta curves). Points A–C indicate a switch on the driving mechanism (overionization-induced refraction, channel guiding, diffraction, and relativistic self-focusing, respectively).

The observed behavior is explained with our composite model. Figure 4 shows the maximum intensity as given by the PIC simulation (red circles) and our ray-tracing model (red and magenta curves). The points named A–C indicate a switch on the mechanism that drives the temporal evolution of the intensity (overionization-induced refraction, channel guiding, diffraction, and relativistic self-focusing). During the first one and a half Rayleigh length the strong density gradient created by the overionization of the plasma refracts the pulse, reducing its intensity. The two parabola model [Eqs. (9) and (10)] mimics this behavior (depicted as a red line in Fig. 4) from $Z = 0$ until $Z \approx 1.5Z_R$ (i.e., point A). From this point (A), the intensity is low, and only the Kr^{8+} ion is maintained in the channel [Fig. 2(b)]. The mechanism that drives the propagation of the pulse is the channel guiding, modeled with one parabola [Eq. (3)] and depicted as a magenta line in Fig. 4. Between points B and C, the one parabola model focuses the beam more than observed in the PIC simulation. As shown in Table I, diffraction and refraction focusing both play a role in the unperturbed channel ($Z_R = 0.0725$ and $Z_1 = 0.11$ cm). However, our model does not take into account diffraction. Thus, the origin of this discrepancy is the switch

of the channel-guiding mechanism (between points A and B) to a competition between guiding and diffraction. At point C ($Z \approx 3Z_R$) the threshold for self-focusing is attained, and the intensity increases (driven by another mechanism, relativistic self-focusing) until overionization again refracts the pulse. Then, the intensity adjusts itself to the value that is guided in the channel, i.e., the one sustaining only Kr^{8+} ions [Figs. 2(a) and 2(b)].

Figure 4 (black diamonds) shows for comparison the case where $n_{e1} = 1.4 \times 10^{16}$ cm^{-3}. In this case, the refraction characteristic length for both overionization refraction ($Z_0 =$ 0.33 cm) and channel focusing ($Z_1 = 1.1$ cm) are much larger than the Rayleigh length ($Z_R = 0.0725$ cm), and thus the propagation is dominated by diffraction. The comparison with a Gaussian beam propagating in vacuum is shown in Fig. 4 (black line).

The *breathing* effect described above has several similitudes and differences with the laser filamentation of intense IR pulses propagating through different media [27,32]. Both mechanisms rely on a focusing effect (optical Kerr effect in the case of laser filamentation and guiding and relativistic self-focusing in this article) and a defocusing effect (ionization induced by the field via multiphoton absorption or tunneling). The differences appear in the range of power and intensities involved on these effects. Whereas both the optical Kerr effect and the relativistic self-focusing are threshold effects, their threshold power and thus the propagated intensity are different by orders of magnitude. The self-focusing threshold in laser filamentation is [33] $P_{\text{th}} = 3.72 \frac{\lambda_0^2}{8\pi n_0 n_2}$, where n_0 is the linear index of refraction and n_2 is the second-order nonlinear index coefficient. For a $\lambda_0 = 800$ nm laser propagating in air at atmospheric pressure, $P_{\text{th}} = 3.2$ GW, and the propagated intensity is on the order of 4×10^{13} W/cm^2 [32,34]. On the other hand, the relativistic self-focusing threshold is [23] $P_{\text{th}} \approx 17 \frac{n_c}{n_e}$ GW. Since usually $n_e \ll n_c$ the latter threshold will be greater than the former (i.e., for $n_e = 0.1 n_c$, a relatively high electron density $P_{\text{th}} = 0.17$ TW). Figures 2(a) and 4 show that the propagated intensity is greater than 10^{17} W/cm^2.

IV. CONCLUSIONS

In this paper we model the propagation of intense ($I > 10^{18}$ W cm^{-2}) IR pulses through dense plasma channels formed by partially ionized high-Z elements (krypton in this article). The propagation of these pulses is highly nonlinear since they are intense enough to locally ionize several times ($\bar{Z} \approx 16$) the atoms, creating steep density gradients. In addition to this, the high electron density achieved reduces the self-focusing threshold, adding complexity to the problem. Unlike in other applications, both high-Z elements and high electron density are required to achieve ultrashort and energetic plasma-based soft-x-ray lasers, and thus a thorough study is needed.

We have shown that efficient guiding of intense IR pulses through dense plasma channels is regulated by two counterbalancing effects. Overionization-induced refraction decreases the intensity of the IR beam over the first Rayleigh length such that only Kr^{8+} ions are present afterwards. From this moment, feedback between waveguide refraction and self-focusing on one side and overionization-induced refraction on the other allows for the guiding of the IR beam and the creation of an almost uniform population of Kr^{8+} ions during several Rayleigh lengths. A better understanding of the waveguide formation along with a thorough parametric study of its experimental implementation should feed the ambition to guide at higher densities and over longer distances. The perspective of guiding at higher densities holds the promise of developing plasma-based x-ray lasers as a worthwhile complementary, and possibly alternative, tool for large-scale and expensive facilities delivering ultraintense coherent x rays.

ACKNOWLEDGMENTS

This work was supported by the Agence Nationale de la Recherche, through Project No. ROLEX ANR-06-BLAN-04 023 01.

[1] H. N. Chapman and K. A. Nugent, Coherent lensless X-ray imaging, Nat. Photonics **4**, 833 (2010).

[2] A. P. Mancuso, T. Gorniak, F. Staier, O. M. Yefanov, R. Barth, C. Christophis, B. Reime, J. Gulden, A. Singer, M. E. Pettit, T. Nisius, T. Wilhein, C. Gutt, G. Grübel, N. Guerassimova, R. Treusch, J. Feldhaus, S. Eisebitt, E. Weckert, M. Grunze, A. Rosenhahn, and I. A. Vartanyants, Coherent imaging of biological samples with femtosecond pulses at the free-electron laser FLASH, New J. Phys. **12**, 035003 (2010).

[3] P. Zeitoun, G. Faivre, S. Sebban, T. Mocek, A. Hallou, M. Fajardo, D. Aubert, P. Balcou, F. Burgy, D. Douillet, S. Kazamias, G. de Lachèze-Muriel, T. Lefrou, S. le Pape, P. Mercère, H. Merdji, A. S. Morlens, J. P. Rousseau, and C. Valentin, A high-intensity highly coherent soft x-ray femtosecond laser seeded by a high harmonic beam, Nature (London) **431**, 426 (2004).

[4] Y. Wang, E. Granados, F. Pedaci, D. Alessi, B. M. Luther, M. Berrill, and J. J. Rocca, Phase-coherent, injection-seeded, table-top soft-x-ray lasers at 18.9 nm and 13.9 nm, Nat. Photonics **2**, 94 (2008).

[5] Y. Wang, M. Berrill, F. Pedaci, M. M. Shakya, S. Gilbertson, Z. Chang, E. Granados, B. M. Luther, M. A. Larotonda, and J. J. Rocca, Measurement of 1-ps soft-x-ray laser pulses from an injection-seeded plasma amplifier, Phys. Rev. A **79**, 023810 (2009).

[6] L. Li, Y. Wang, S. Wang, E. Oliva, L. Yin, T. T. T. Le, S. Daboussi, D. Ros, G. Maynard, S. Sebban, B. Hu, J. J. Rocca, and P. Zeitoun, Wavefront improvement in an injection-seeded soft x-ray laser based on a solid-target plasma amplifier, Opt. Lett. **38**, 4011 (2013).

[7] E. Oliva, M. Fajardo, L. Li, S. Sebban, D. Ros, and P. Zeitoun, Soft x-ray plasma-based seeded multistage amplification chain, Opt. Lett. **37**, 4341 (2012).

[8] E. Oliva, M. Fajardo, L. Li, M. Pittman, T. T. T. Le, J. Gautier, G. Lambert, P. Velarde, D. Ros, S. Sebban, and P. Zeitoun, A proposal for multi-tens of GW fully coherent femtosecond soft x-ray lasers, Nat. Photonics **6**, 764 (2012).

[9] F. Tissandier, S. Sebban, J. Gautier, P. Zeitoun, E. Oliva, A. Rousse, and G. Maynard, Three-dimensional Maxwell-Bloch calculation of the temporal profile of a seeded soft x-ray laser pulse, Appl. Phys. Lett. **101**, 251112 (2012).

[10] O. Larroche and A. Klisnick, Two-dimensional Maxwell-Bloch simulation of quasi-π-pulse amplification in a seeded XUV laser, Phys. Rev. A **88**, 033815 (2013).

[11] D. S. Whittaker, M. Fajardo, P. Zeitoun, J. Gautier, E. Oliva, S. Sebban, and P. Velarde, Producing ultrashort, ultraintense plasma-based soft-x-ray laser pulses by high-harmonic seeding, Phys. Rev. A **81**, 043836 (2010).

[12] B. E. Lemoff, C. P. J. Barty, and S. E. Harris, Femtosecond-pulse-driven, electron-excited XUV lasers in eight-times-ionized noble gases, Opt. Lett. **19**, 569 (1994).

[13] B. E. Lemoff, G. Y. Yin, C. L. Gordon III, C. P. J. Barty, and S. E. Harris, Demonstration of a 10-Hz Femtosecond-Pulse-Driven XUV Laser at 41.8 nm in Xe IX, Phys. Rev. Lett. **74**, 1574 (1995).

[14] R. Keenan, J. Dunn, P. K. Patel, D. F. Price, R. F. Smith, and V. N. Shlyaptsev, High-Repetition-Rate Grazing-Incidence Pumped X-Ray Laser Operating at 18.9 nm, Phys. Rev. Lett. **94**, 103901 (2005).

[15] R. Rankin, N. H. Burnett, P. B. Corkum, and C. E. Capjack, Refraction effects associated with multiphoton ionization and ultrashort-pulse laser propagation in plasma waveguides, Opt. Lett. **16**, 835 (1991).

[16] C. G. Durfee and H. M. Milchberg, Light pipe for high intensity laser pulses, Phys. Rev. Lett. **71**, 2409 (1993).

[17] W. P. Leemans, B. Nagler, A. J. Gonsalves, C. Tóth, K. Nakamura, C. G. R. Geddes, E. Esarey, C. B. Schroeder, and S. M. Hooker, GeV electron beams from a centimetre-scale accelerator, Nat. Phys. **2**, 696 (2006).

[18] M.-C. Chou, P.-H. Lin, C.-A. Lin, J.-Y. Lin, J. Wang, and S.-Y. Chen, Dramatic Enhancement of Optical-Field-Ionization Collisional-Excitation X-Ray Lasing by an Optically Preformed Plasma Waveguide, Phys. Rev. Lett. **99**, 063904 (2007).

[19] P.-H. Lin, M.-C. Chou, C.-A. Lin, H.-H. Chu, J.-Y. Lin, J. Wang, and S.-Y. Chen, Optical-field-ionization collisional-excitation x-ray lasers with an optically preformed plasma waveguide, Phys. Rev. A **76**, 053817 (2007).

[20] A. M. Perelomov, V. S. Popov, and M. V. Terent'ev, Ionization of atoms in an alternating electric field, J. Exp. Theor. Phys. **23**, 924 (1966).

[21] M. V. Ammosov, N. B. Delone, and V. P. Krainov, Tunnel ionization of complex atoms and of atomic ions in an alternating electromagnetic field, J. Exp. Theor. Phys. **64**, 1191 (1986).

[22] C. E. Max, J. Arons, and A. B. Langdon, Self-Modulation and Self-Focusing of Electromagnetic Waves in Plasmas, Phys. Rev. Lett. **33**, 209 (1974).

[23] P. Sprangle, C.-M. Tang, and E. Esarey, Relativistic Self-Focusing of Short-Pulse Radiation Beams in Plasmas, IEEE Trans. Plasma Sci. **15**, 145 (1987).

[24] B. S. Paradkar, B. Cros, P. Mora, and G. Maynard, Numerical modeling of multi-GeV laser wakefield electron acceleration inside a dielectric capillary tube, Phys. Plasmas **20**, 083120 (2013).

[25] P. Mora and T. M. Antonsen, Jr., Kinetic modeling of intense, short laser pulses propagating in tenuous plasmas, Phys. Plasmas **4**, 217 (1997).

[26] S. Sebban, T. Mocek, D. Ros, L. Upcraft, P. Balcou, R. Haroutunian, G. Grillon, B. Rus, A. Klisnick, A. Carillon, G. Jamelot, C. Valentin, A. Rousse, J. P. Rousseau, L. Notebaert, M. Pittman, and D. Hulin, Demonstration of a Ni-Like Kr Optical-Field-Ionization Collisional Soft X-Ray Laser at 32.8 nm, Phys. Rev. Lett. **89**, 253901 (2002).

[27] A. Couairon and A. Mysyrowicz, Femtosecond filamentation in transparent media, Phys. Rep. **441**, 47 (2007).

[28] Y.-F. Xiao, H.-H. Chu, H.-E. Tsai, C.-H. Lee, J.-Y. Lin, J. Wang, and S.-Y. Chen, Efficient generation of extended plasma waveguides with the axicon ignitor-heater scheme, Phys. Plasmas **11**, L21 (2004).

[29] F. Tissandier, Caractérisation spatio-temporelle d'une chaîne laser à 32.8 nm par plasma laser et perspectives vers une source untrabrève et intense, Ph.D. thesis, Ecole Polytechnique, 2011.

[30] F. Tissandier, S. Sebban, M. Kozlova, J. Gautier, P. Zeitoun, A. Klisnick, and G. Maynard, High Density Optical-Field-Ionization Soft X-Ray Lasers, in *X-Ray Lasers 2012*, edited by S. Sebban, J. Gautier, D. Ros, and P. Zeitoun, Springer Proceedings in Physics Vol. 147 (Springer, Berlin, 2014), pp. 243–255.

[31] E. E. Fill, Ray trajectories in line-focused laser plasmas, J. Opt. Soc. Am. B **14**, 1505 (1997).

[32] S. L. Chin, The physics and the challenge of the propagation of powerful femtosecond laser pulses in optical media, Phys. Canada **60**, 273 (2004).

[33] J. Marburger, Self-focusing: Theory, Progr. Quantum Electron. **4**, 35 (1975).

[34] J. Kasparian, R. Sauerbrey, and S. Chin, The critical laser intensity of self-guided light filaments in air, Appl. Phys. B **71**, 877 (2000).